Structural deformation of metallic uranium surrounding hydride growth sites

Christopher P. Jones[a], Thomas B. Scott[a,*], James R. Petherbridge[b].

[a]Interface Analysis Centre, University of Bristol, 121 St Michael's Hill, Bristol, BS2 8BS, UK

[b]AWE, Aldermaston, Reading, Berkshire, RG7 4PR, UK

ABSTRACT

Electron backscatter diffraction (EBSD) was utilised to probe the microstructure of uranium metal in the vicinity of surface corrosion pits, resulting from hydrogen exposure (5×10^4 Pa, at 240°C). Microstructural analysis of the surface revealed a subtle increase of grain orientation variation for grains at the border of the hydride growths. Cross sectional analysis, at pit sites, revealed significant microstructure deformation in the form of crystal twinning and micro-cracking beneath the surface. These observations provide qualitative evidence that local stress intensities generated as a consequence of hydride growth and confinement, were sufficient to cause deformation within the parent metal.

* Corresponding author: email cj0810@bristol.ac.uk Tel: 44 117 3311176

1. INTRODUCTION

Uranium is vulnerable to corrosion by environmental gases that may lead to material degradation, shortened lifetimes, alteration of mechanical properties and ultimately material failure. This is particularly apparent in the case of corrosion by hydrogen where the primary reaction product, hydride (UH_3), is both pyrophoric and has significantly lower density than the metal at room temperature (10.95 g cm^{-3} and 19.1 g cm^{-3}, respectively). Consequently, a fundamental understanding of the corrosion process at all stages is of critical importance.

Typically, it is observed that, at a given temperature, the reaction proceeds when the metal is exposed to H_2 at a pressure which exceeds the equilibrium pressure of the metal hydride (UH_3). This leads to a direct solid-gas interaction in which the metal is converted to the hydride. Initial reaction takes the form of discrete hydride nucleation sites forming across the metal surface [1, 2]. With continued corrosion these sites are reported to grow and ultimately coalesce, forming an encompassing film of hydride, prone to spallation as a fine pyrophoric powder [3-5]. The arising powder has been characterised as UH_3 using X-ray photoelectron spectroscopy [6] and X-ray diffraction [3].

Many published studies have primarily focused on measuring the kinetics of the reaction, i.e. the rate at which reaction sites nucleate or the overall rate of reaction [2, 7-17]. However, advances in surface analysis techniques have allowed the influence of bulk and surface properties of uranium metal to be investigated. Thus, hydride site initiation has been correlated with metallic defect sites such as grain boundaries, scratches, inclusion (carbide) particles, and crystal twins [1, 5, 6, 18-26].

Indeed, previous studies reported by the current authors have indicated that material in which there is a high surface concentration of carbide inclusion particles (i.e. 575 inclusions per mm^2 for uranium with a carbon concentration of 600ppm) exhibit a marked preference for hydride forming reactions to occur at these inclusion sites [19]. However, in the case of high purity uranium in which the surface concentration of inclusion sites is much lower (i.e. ~20 inclusions per mm^2 for material with a carbon content of <100 ppm) nucleation of hydride formation sites is predominantly observed at metal grain boundaries [1, 24]. These observations would seem to suggest that inclusions provide a more favorable location for hydride reaction to initiate, as compared to metal grain boundaries, and that the latter only become significant when the former are present at very low concentrations.

Such observations are consistent, to some extent, with a model in which the surface oxide layer present on the uranium metal surface presents a barrier that hydrogen must breach in order to reach the underlying metal [4, 27]. For instance, inclusions exposed at the metal surface interrupt the overlying uranium oxide layer and could thus provide express pathways for hydrogen diffusion, as suggested by Harker et al. [19]. However, the precise causes for the preferential hydride nucleation observed at inclusions and grain boundaries are still to be discerned.

Although a number of studies have been reported [11-13, 15], the exact details of the mechanism by which a hydride reaction site grows into the surrounding uranium metal still remains uncertain. What is clear is that once a hydride reaction site has nucleated and expanded to such an extent that the surface oxide layer is breached, the growth rate of the site increases dramatically. Partially, this is ascribed to the diffusion of hydrogen through the hydride at an established reaction site being far more rapid than the diffusion through the surface oxide layer (as required for the nucleation of a new site).

In conclusion, it can be stated that, a number of outstanding questions remain related to the underlying causes of the reported preferential hydride site growth at metal grain boundaries and inclusion particles. In addition, the mechanism by which these sites grow is still yet to be fully understood. Therefore, the primary goal of the current research was to provide a better understanding of the initial stages of hydrogen corrosion on uranium surfaces by identifying and investigating any structural changes occurring in the metal surrounding hydride growth sites. Specifically, the following work investigated how the stresses generated by hydride growth are accommodated by the surrounding microstructure of the metal, both at the metal surface and within the bulk. This was achieved using new focused ion beam (FIB) surface preparation techniques suitable for successful EBSD analysis of large scale (>10μm) hydride growths. The as received samples were annealed in order to promote both grain growth and the relaxation of the residual internal stresses present in the material, thereby generating a cleaner, simpler, microstructure prior to hydriding. Also, it should be noted that in order to minimise the possible influence of carbide inclusions on observed hydride site nucleation the current work used uranium material with a low carbon content (<100 ppm).

2. EXPERIMENTAL

2.1 Initial surface preparation and subsequent formation of hydrides

Sample coupons (10 mm square, ~1 mm thick) were obtained from rolled depleted uranium feedstock with a grain size of ~15μm. Chemical analysis of samples from the same source [28] yielded impurity levels for carbon, aluminium, iron, silicon and chromium of ~50, 22, ~5, ~2 and ~2 ppm (by weight), respectively. These samples were annealed under UHV conditions (<$1\times10^{-}$

^{4}Pa) at 550°C for 9 days in order to minimise residual internal stresses and promote grain growth. The annealing of the high purity metal was invoked to provide a material with few crystalline defects and low residual stress upon which to observe orientation changes induced by controlled hydride growth. The samples were prepared in the open laboratory by wet mechanical polishing. Samples were sequentially abraded using Buehler SiC paper of increasingly fine grade to P4000 grit, producing a 2-3 μm surface finish. Samples were then lapped using 1μm diamond paste in an argon filled glovebox, rinsed and washed clean using research grade ethanol prior to electropolishing. The aim of the electropolishing step was to remove the majority of surface topographical anomalies, such as microscratches, thus reducing the number of possible preferential nucleation sites. The process used an electrolyte solution consisting of a 10:6:6 ratio by volume of research grade ethanol, orthophosphoric acid (85%) and ethylene glycol, respectively. The electrolyte was contained within a stainless steel beaker (acting as a cathode) and a variable voltage was applied to maintain a current of 0.2 A. The samples were electropolished for 5 minutes, rinsed in absolute ethanol, passivated by a short immersion (2-3 seconds) in the unbiased electrolyte, rinsed again in ethanol then air dried using a blower system.

The samples were then immediately gasket-sealed into a half-inch diameter stainless steel Swagelok vacuum cell with built-in thermocouple. The cell was evacuated to a pressure lower than 5×10^{-4} Pa and subsequently heated to (and maintained at) 75°C for 12 hour duration to drive off adsorbed water from the sample surface. The cell was then heated to the desired reaction temperature of 240°C where it was maintained for two hours to reach thermal equilibrium, and drive off any residual surface adsorbed water, prior to the introduction of hydrogen gas. Purified hydrogen (from a lanthanum-nickel hydride bed) was added to the reaction cell and a section of the rig (72.6 cm^3 total volume) at a pressure of 5×10^{4} Pa. Upon sealing this volume, the gas

pressure was monitored to observe the onset of hydride formation and halted (by evacuation of gas via a rotary pump) after a 500-1500 Pa drop was recorded, equivalent to reaction of approximately 1% of the sample. Samples were then allowed to cool to room temperature under UHV conditions before precursory analysis.

Microscopy confirmed that the resulting samples had undergone limited hydride formation with a low number (<30) of hydride nucleation sites observed across the entirety of the coupon's surface. The fully formed hydrides were observed to range in surface diameter from 35 µm to 120 µm (Figure 1). Assuming that the growth sites all share a similar growth rate, the observed range in hydride size indicates that the growths did not initiate simultaneously during the hydrogen exposure.

2.2 Mechanical cross-section and preparation for EBSD analysis

EBSD analysis of the hydride inclusions was conducted both at the surface of the uranium and on a mechanically prepared cross-section through the hydride (and surrounding metal). For surface investigation of the metal microstructure, electropolishing (30-60 seconds duration) was conducted following the procedure described in section 2.1. This etched ~10nm of material, removing any surface formed oxide layer whilst leaving the morphology of the hydride growth sites ostensibly unaltered. The resulting sample surface was uniformly smooth, enabling microstructural characterisation via EBSD analysis to be performed.

However, the use of EBSD to probe the sub-surface metal surrounding the hydride growth sites required sufficient sample material to be removed in order for the backscattered electrons to reach the detector without reabsorption. This was achieved by first mechanically sectioning a hydride

coupon adjacent to a hydride site. The cut surface was then gradually abraded back, using P1200 grade SiC paper, until the hydride site was intersected. For both the sample surface (in the case of lateral growth investigation) and the cross-section face (for a vertical, subsurface, investigation), the uranium metal adjacent to the hydride growth site was prepared for EBSD analysis via the same process described in section 2.1, culminating in electrochemical etching. Figure 2 shows a hydride crater after electropolishing the newly exposed face. The metal grains surrounding the pit are clearly visible from the SEM image due to differential channelling contrast caused by variation in crystallographic orientation.

For detailed subsurface investigation of the uranium metal in the immediate vicinity of the hydride growths, focussed ion beam (FIB) milling was required because the electropolishing process had preferentially etched the fine features from the hydride-metal boundary (regions of high localised current density are generated around protruding artefacts on the sample surface). FIB milling was performed using a FEI FIB-201 with a liquid gallium ion source operating at 30kV with the maximum available probe current (11 nA), and the beam skimming at 90° to the exposed surface. This produced a high quality surface for EBSD analysis, albeit in a limited area adjacent to the hydride growth.

3. RESULTS

3.1 Hydride surface number density

FIB imaging of the reacted samples revealed very few hydride growth sites on the sample surface, a total of 24 being found in a 10 mm x 10 mm area. The low number density of growth sites coupled with the degree of hydrogen consumed (1×10^3 Pa) meant that the individual growths were

typically between 35 and 120 μm in diameter (Figure 1). The surface was electropolished to remove any micro-structural damage in the metal generated by mechanical abrasion and any surface topographic anomalies and oxide formed in the interim period. The result is a surface with few preferential nucleation sites and a very thin uniform oxide. Consequently only limited numbers of hydrides are observed to form, which will grow to substantial sizes (>500 μm surface diameter) without significant generation of new nucleation sites to provide competition for H_2 uptake.

3.2 Analysis of surface hydride growths

Figure 1 shows four FIB rastered secondary electron images of typical hydride growths at the surface of uranium metal. Hydrides typically exhibited a circular morphology (a-c) although evidence of elongated or angular morphology (d) was also present. The metal microstructure surrounding the hydride sites was revealed using FIB grazing angle etching, at an 80° angle of incidence, which removed the surface oxide formed after electropolishing was performed. The FIB instrument was also used to generate high contrast secondary electron images, revealing the grain microstructure, of the uranium metal surrounding hydride craters.

An inverse pole figure (IPF) crystallographic orientation map (Figure 3a) was produced from lateral EBSD surface analysis with complementary information drawn from secondary electron images recorded from the hydride areas (Figure 3b). Surface areas of exposed hydride or oxide did not yield diffraction patterns strong enough for indexing. This was ascribed to significant topographic variation and/or crystallite sizes too small for the EBSD to map correctly. These regions could not be indexed and thus display as noise in the crystallographic orientation maps.

At the surface of the coupon, evidence for ductile deformation within the metal bordering hydride growths was investigated by analysis of orientation variation within individual metal grains. For each grain, internal variation in crystallographic orientation was plotted for values up to 10° about the grain average orientation (Figure 3c). Comparison of the data with that recorded from non-hydrided material of the same type (Figure 3d), indicated that the internal crystallographic variation differed significantly for a few locations at the border of the hydride metal interface, extending up to 15μm across the surface. However, the majority of the sample, even within 1μm of the hydride growth, exhibited no significant signs of internal stress when compared to the surface of non-hydrided metal coupons of the same provenance. Features such as radial micro-cracks extending into the metal from the hydride margins were expected to provide evidence of brittle deformation in response to hydriding. However, at the coupon surface, no such evidence was obtained from the current work.

3.3 Cross-section investigation of hydride growths

Converse to the study of the metal surface, the cross-sectional investigation of the uranium surrounding hydride growth sites revealed a more significant alteration of the microstructure. Although the hydride powder produced by the reaction between hydrogen and uranium is not confined (i.e. is free to spill out of the corrosion pit), and thus cannot generate large levels of macroscopic hydraulic strain, it is reasonable to assume that inhomogeneous hydride growth at the metal:hydride reaction interface would lead to areas where local stress intensities could be significant. Such local stress intensities would be generated by the growth of hydride within small confined areas at the metal:hydride interface.

Since the observed deformation at the metal surface was negligible, a cross-sectional crystallographic analysis of the unreacted metal immediately surrounding a number of hydride growths was warranted. To achieve this, the metal was sectioned at the location of a hydride growth and the freshly revealed face prepared via electropolishing and then FIB etching for EBSD analysis.

The grain structure of the metal in the vicinity of an example hydride growth site is displayed as a crystallographic orientation (IPF) map for a sample prepared only via electropolishing, with each instance of crystalline twinning labelled (Figure 4). The metal grains in the immediate vicinity (<1 μm) of the hydride were not successfully mapped due to the preferential etching that the electropolishing process induces, thereby removing any fine interfacial features that may have been present. Adjacent to this region, extensive twinning was observed within the metal grains in the vicinity of the hydride crater. This grain slipping phenomena has been regularly observed as a release mechanism for the build-up of internal stresses within the metal [29]. In this instance the stresses were confined (in contrast to the coupon surface) and distortion in the crystal grains was clearly evident by the emergent crystal twins. It should be noted that areas remote from the hydride reaction site exhibit twinning due to the sample manufacturing process; however, 59% of the twins present originate within 50μm of the hydride crater. Therefore, the number density of twins in the 50μm adjacent to the crater is 2.59×10^{-3} μm^{-2}, as compared to 7.46×10^{-4} μm^{-2} for the remaining area that was analysed (i.e. a difference of a factor of ~3.5).

To investigate, in greater detail, the metallic structure within the immediate vicinity of the hydride crater, FIB etching of the hydride site was required prior to EBSD analysis. The resulting grain structure (Figure 5) highlights the influence that the growing hydride exerted on neighbouring metal grains with regions of particular interest enlarged in figures 5a-d. Several maps were taken,

and all indicated a significant amount of lenticular twinning in grains immediately abutting the hydride growths (Figure 5a-c).

The EBSD maps prepared by FIB milling also showed potential evidence of fragmentation (Figure 5b) and microcracking (Figure 5d) in close proximity to the hydride pit. Figure 6 provides arguably clearer evidence of microcracking by presenting analysis obtained following focused ion milling using a low beam current in order to limit any induced surface damage. The features observed give some indication that localised stresses were present in the uranium metal, ascribed to strain generated by hydride growth.

The regions not mapped successfully were ascribed to areas where hydride was present. Figure 5b displays fragments of uranium metal that were detected within the growing hydride body. These fragments had been isolated from the rest of the metal during rapid hydride growth but had not been fully consumed by the time the reaction was halted.

Figure 7 presents qualitatively the distortions within individual metal grains by selecting four grains at successively greater distances from the edge of a hydride growth. The inverse pole plots are isolated for each grain to show the variation in crystallographic orientation relative to the grain average. Each point plotted on the IPF corresponds to the orientation of a point within the grain, therefore, a tight bundle of points indicates uniformity in crystallographic orientation across, and thus minimal distortion of, the grain. Conversely, a diffuse grouping of points for a given grain on the IPF corresponds to a large range of crystalline orientations, and thus high levels of distortion within the grain. It is clear that the grains in close proximity to the hydride (1 and 2) exhibited a lower congruency than those at a distance (3 and 4). This qualitative result provides evidence that the crystal lattice of the metal grains has been significantly distorted, and it is assumed that this

was due to the stresses generated by the hydride expansion exerting compressive stresses into the individual grains.

4. DISCUSSION

With regard to the nucleation of the hydride reaction siters investigated, deliberate electropolishing of the metal surface, prior to hydriding, resulted in a low number of large hydrides. The low number of new nucleation sites appearing, after the initial growth sites are well established, is associated with both the energetics and kinetics of the processes governing existing site growth or new site nucleation. The processes associated with the growth of existing sites are either low energy (dissociation on hydride) or rapid (diffusion through hydride), whilst those associated with the nucleation of new sites occur less readily (dissociation on oxide surface) and are slower (diffusion through oxide). In each case, these processes determine how rapidly the hydrogen concentration in the underlying metal increases with time and approaches that required for the precipitation of hydride.

Microstructural analysis of the metal surface revealed a preferred orientation in the metal towards the [001] direction. This corresponds with previous studies that have ascribed this texture to be a product of low-temperature rolling during manufacturing. In the current study, evidence of preferential hydride propagation into grains of a particular orientation was inconclusive. Whilst there appeared to be more rapid hydride propagation into grains closer to the [100] orientation, the data indicated a greater tendency for preferential propagation to occur through the smaller metal grains and along grain-boundaries (Figure 3a-c). In addition, there was clear evidence of subtle,

small scale, deformation of the uranium metal in discreet locations immediately surrounding the hydride sites.

Therefore, the lack of obvious surface damage or deformation suggests that the hydraulic stresses induced by hydride growth at the surface of the material are either; i) insufficient to induce ductile and/or brittle deformation of the metal, because the hydride is instead expanding outwards from the sample surface where it is unconfined, or ii) accommodated by the grain structure of the metal via 'slip' type movements along grain boundary networks. As it stands, the hydride appears to only impart crystalline deformation into a select few grains that are in the process of being consumed by the hydride expansion.

Analysis of the metal subsurface region bounding hydride growths provided more substantial evidence of subsurface deformation of the metal caused by hydride expansion (Figures 4-6). The data presented in Figure 7 provided an indication of the stresses induced by the hydride by revealing residual deformation structures produced within the parent metal. Taking the formation of crystal twins as the prime example, it is recognised that shear twinning is a key mechanism for the accommodation of mechanical stresses in uranium. In the current work instances of twinning, characterised by a 69° rotation about the <001> axis relative to the parent grain, were most frequently observed as stress induced deformations in the metal bordering hydride growths. This indicates that stresses imposed on the metal grains immediately adjoining a hydride growth centre exceeded the threshold value required for the initiation of twinning, i.e. 0.024 Kg mm^{-2} as reported for 600°C by Chiswik et al [30].

Incidences of crystal twinning were most numerous within a zone 50-80 μm from the hydride margins compared to elsewhere in the metal, and many of the twins observed in these zones were

malformed and ran discontinuously across their parent grains. The twin malformation observed is assumed to relate to both rapid and incomplete deformation, with cessation of straining as the hydriding reaction was halted. Induced stresses are considered to be relieved by several modes, with twinning and microcracking being the two most readily observed phenomena. Slipping along grain boundaries congruent to stresses produced from hydride expansion is also believed to occur, however, this was not detectable by the techniques employed here.

The presence of micro-cracking was only observed in the subsurface region of the metal (Figures 5d and 6) where hydraulic pressure caused by the expansion of the hydride sites was considered to be far greater than at the sample surface. From the EBSD data presented in Figure 6, discontinuities ascribed to micro-cracking were observed to follow irregular pathways through individual grains and EBSD plots of crystal orientation variation clearly indicate an associated distortion of the bounding metal by an angular variation of up to 10º. Fragments of uranium metal were also detected within the growing hydride body (Figure 5b) suggesting that the hydride can, and does, form rapidly around grain margins [24] causing the break off of metal grains into the propagating hydride mass. These isolated grain fragments would probably be consumed by continued hydride formation. Presumably, the high stresses required for these phenomenon were generated by material confinement at the expanding hydride edge, where the available routes for pressure relief are minimal when compared with the near surface region.

On first examination, it seems counterintuitive that a hemispherical hydride reaction site in which the product hydride powder was unconstrained would induce stress into the surrounding metal. However, a study reported by Greenbaum et al [31] modelled the elastic fields setup by a semi-spherical hydride particle growing on a free surface of a metal with cubic symmetry, and concluded that regions of tensile and compressive hydrostatic stress were indeed generated in the

surrounding matrix. The work of Greenbaum et al therefore provides a further indication that in the present study internal stresses were generated leading to localised brittle failure of the metal; likely exploiting pre-existing structural weaknesses. However, it should be noted that the model used by Greenbaum et al did not consider grain boundaries nor the observed behaviour of preferential hydride growth at these locations.

Previous work [24] has indicated that hydride sites can be 'self-propagating' in terms of forcing apart grain boundaries, at which they form, to provide preferential low pressure zones for formation. Growths can thus propagate into the bulk of the metal by inducing micro-cracking and fragmentation of subsurface metal grains, thereby providing low pressure zones for H_2 accumulation and further hydride precipitation, a self-perpetuating process. During hydride formation in the metal, stresses are expected to initially relieve through the process of grain boundaries slipping. However, slipping along grain boundaries does not produce identifiable features and the only method of identifying this phenomenon is through a comparison with an accurate microstructural picture of the surface prior to hydrogen exposure to identify subtle, relative, changes between grain positions.

Future work examining the magnitude and distribution of stresses in the metal surrounding the hydride growth sites and for different uranium microstructures will provide further insight into the nature of the deformations observed in the current work. It is suggested that cross-correlation EBSD and digital image correlation (DIC) are potentially powerful tools for quantitatively mapping residual stresses across a surface which would provide a logical means of gaining this information. A nano-indentation hardness map of the metal surrounding a sectioned hydride site might also be of value.

5. CONCLUSIONS

The current research has examined the mechanical response of rolled low-carbon uranium to the growth of hydride at point locations on the metal surface. On the metal surface evidence of subtle grain deformation was observed indicating microstructural accommodation of stresses generated by hydride growth. In contrast, investigation of microstructural deformation deeper into the metal revealed extensive twinning and limited evidence of micro-cracking in the grains immediately adjacent to hydride growth sites. Additionally, the recorded internal variation in crystallographic orientation within individual grains was significantly higher for grains abutting hydride growths than for grains in the unaffected parent metal.

The cumulative effect of hydride growth was the formation of preferred pathways for hydrogen diffusion as the bulk metal responded to the localised stresses induced by hydride formation. This resulted in a preference for further growth of existing hydride sites over nucleation of new growth centres on the electropolished uranium surface.

REFRENCES

1. C.P. Jones, T.B. Scott, J.R. Petherbridge, J. Glascott, A surface science study of the initial stages of hydrogen corrosion on uranium metal and the role played by grain microstructure, Solid State Ionics 231 (2013) 81-86.
2. S.G. Bazley, J.R. Petherbridge,J. Glascott, The influence of hydrogen pressure and reaction temperature on the initiation of uranium hydride sites, Solid State Ionics 211 (2012) 1-4.
3. F. Le Guyadec, X. Genin, J.P. Bayle, O. Dugne, A. Duhart-Barone, C. Ablitzer, Pyrophoric behaviour of uranium hydride and uranium powders, Journal of Nuclear Materials 396 (2-3) (2010) 294-302.
4. Y. Ben-Eliyahu, M. Brill, M.H. Mintz, Hydride nucleation and formation of hydride growth centers on oxidized metallic surfaces-kinetic theory, Journal of Chemical Physics 111 (13) (1999) 6053-6060.
5. R. Arkush, A. Venkert, M. Aizenshtein, S. Zalkind, D. Moreno, M. Brill, M.H. Mintz,N. Shamir, Site related nucleation and growth of hydrides on uranium surfaces, Journal of Alloys and Compounds 244 (1-2) (1996) 197-205.
6. G.C. Allen, J.C.H. Stevens, The Behavior of Uranium Metal in Hydrogen Atmospheres, Journal of the Chemical Society-Faraday Transactions I 84 (1988) 165-174.
7. J.E. Burke, C.S. Smith, The formation of uranium hydride, Journal of the American Chemical Society 69 (10) (1947) 2500-2.
8. W.M. Albrecht, M.W. Mallett, Reaction of Hydrogen with Uranium, Journal of The Electrochemical Society 103 (7) (1956) 404-409.
9. E. Wicke, K. Otto, The uranium-hydrogen system and the kinetics of uranium hydride formation, Zeitschrift für Physikalische Chemie 31 (3-4) (1962) 222-248.
10. J.B. Condon, E.A. Larson, Kinetics of the uranium-hydrogen system, The Journal of Chemical Physics 59 (2) (1973) 855-865.
11. J.B. Condon, Calculated Vs Experimental Hydrogen Reaction-Rates with Uranium, Journal of Physical Chemistry 79 (4) (1975) 392-397.
12. J.B. Condon, Nucleation and Growth in the Hydriding Reaction of Uranium, Journal of the Less-Common Metals 73 (1) (1980) 105-112.
13. J. Bloch, M.H. Mintz, Kinetics and Mechanism of the U-H Reaction, Journal of the Less-Common Metals 81 (2) (1981) 301-320.
14. G.L. Powell, W.L. Harper, J.R. Kirkpatrick, The Kinetics of the Hydriding of Uranium Metal, Journal of the Less-Common Metals 172 (1991) 116-123.
15. J.R. Kirkpatrick, J.B. Condon, The Linear Solution for Hydriding of Uranium, Journal of the Less-Common Metals 172 (1991) 124-135.
16. R. Li, X. Wang, Effect of niobium additions on initial hydriding kinetics of uranium, Journal of Nuclear Materials 449 (1–3) (2014) 49-53.
17. P. Shi, L. Shen, B. Bai, D. Lang, L. Lu, G. Li, X. Lai, P. Zhang,X. Wang, Preferred hydride growth orientation of U−0.79 wt.% Ti alloy with $\beta+U_2Ti$ microstructure, Journal of Nuclear Materials 441 (1–3) (2013) 1-5.
18. J.F. Bingert, R.J. Hanrahan, R.D. Field, P.L. Dickerson, Microtextural investigation of hydrided alpha-uranium, Journal of Alloys and Compounds 365 (1-2) (2004) 138-148.

19. N.J. Harker, T.B. Scott, C.P. Jones, J.R. Petherbridge, J. Glascott, Altering the hydriding behaviour of uranium metal by induced oxide penetration around carbo-nitride inclusions, Solid State Ionics 241 (2013) 46-52.
20. D. Moreno, R. Arkush, S. Zalkind, N. Shamir, Physical discontinuities in the surface microstructure of uranium alloys as preferred sites for hydrogen attack, Journal of Nuclear Materials 230 (2) (1996) 181-186.
21. P. Morrall, D.W. Price, A.J. Nelson, W.J. Siekhaus, E. Nelson, K.J. Wu, M. Stratman, W. Mclean, ToF-SIMS characterization of uranium hydride, Philosophical Magazine Letters 87 (8) (2007) 541-547.
22. A.J. Nelson, T.E. Felter, K.J. Wu, C. Evans, J.L. Ferreira, W.J. Sickhaus, W. Mclean, Uranium passivation by C+ implantation: A photoemission and secondary ion mass spectrometry study, Surface Science 600 (6) (2006) 1319-1325.
23. G.L. Powell, A.G. Dobbins, S.S. Cristy, T.L. Cliff, H.M. Meyer, J. Lucania,M. Milosevic, The Study of the Oxidation of Uranium by External and Diffuse-Reflectance Ftir Spectroscopy Using Remote-Sensing and Evacuable Cell Techniques, 9th International Conference on Fourier Transform Spectroscopy 2089 (1993) 214-215.
24. T.B. Scott, G.C. Allen, I. Findlay, J. Glascott, UD_3 formation on uranium: evidence for grain boundary precipitation, Philosophical Magazine 87 (2) (2007) 177-187.
25. T.B. Scott, J.R. Petherbridge, N.J. Harker, R.J. Ball, P.J. Heard, J. Glascott, G.C. Allen, The oxidative corrosion of carbide inclusions at the surface of uranium metal during exposure to water vapour, Journal of Hazardous Materials 195 (2011) 115-123.
26. M.A. Hill, R.K. Schulze, J.F. Bingert, R.D. Field, R.J. Mccabe, P.A. Papin, Filiform-mode hydride corrosion of uranium surfaces, Journal of Nuclear Materials 442 (1–3) (2013) 106-115.
27. J. Glascott, A model for the initiation of reaction sites during the uranium-hydrogen reaction assuming enhanced hydrogen transport through thin areas of surface oxide, Philosophical Magazine 94 (3) (2013) 221-241.
28. R.M. Harker, The influence of oxide thickness on the early stages of the massive uranium-hydrogen reaction, Journal of Alloys and Compounds 426 (1-2) (2006) 106-117.
29. D.M.R. Taplin, On the question of the grain size dependence of the flow and fracture stress in alpha uranium, Journal of Nuclear Materials 19 (2) (1966) 208-209.
30. H.H. Chiswik, A.E. Dwight, L.T. Lloyd, M.V. Nevitt, S.T. Zegler, Advances in the physical metallurgy of uranium and its alloys (1958) 35.
31. Y. Greenbaum, D. Barlam, M.H. Mintz, R.Z. Shneck, Elastic fields generated by a semi-spherical hydride particle on a free surface of a metal and their effect on its growth, Journal of Alloys and Compounds 509 (9) (2011) 4025-4034.

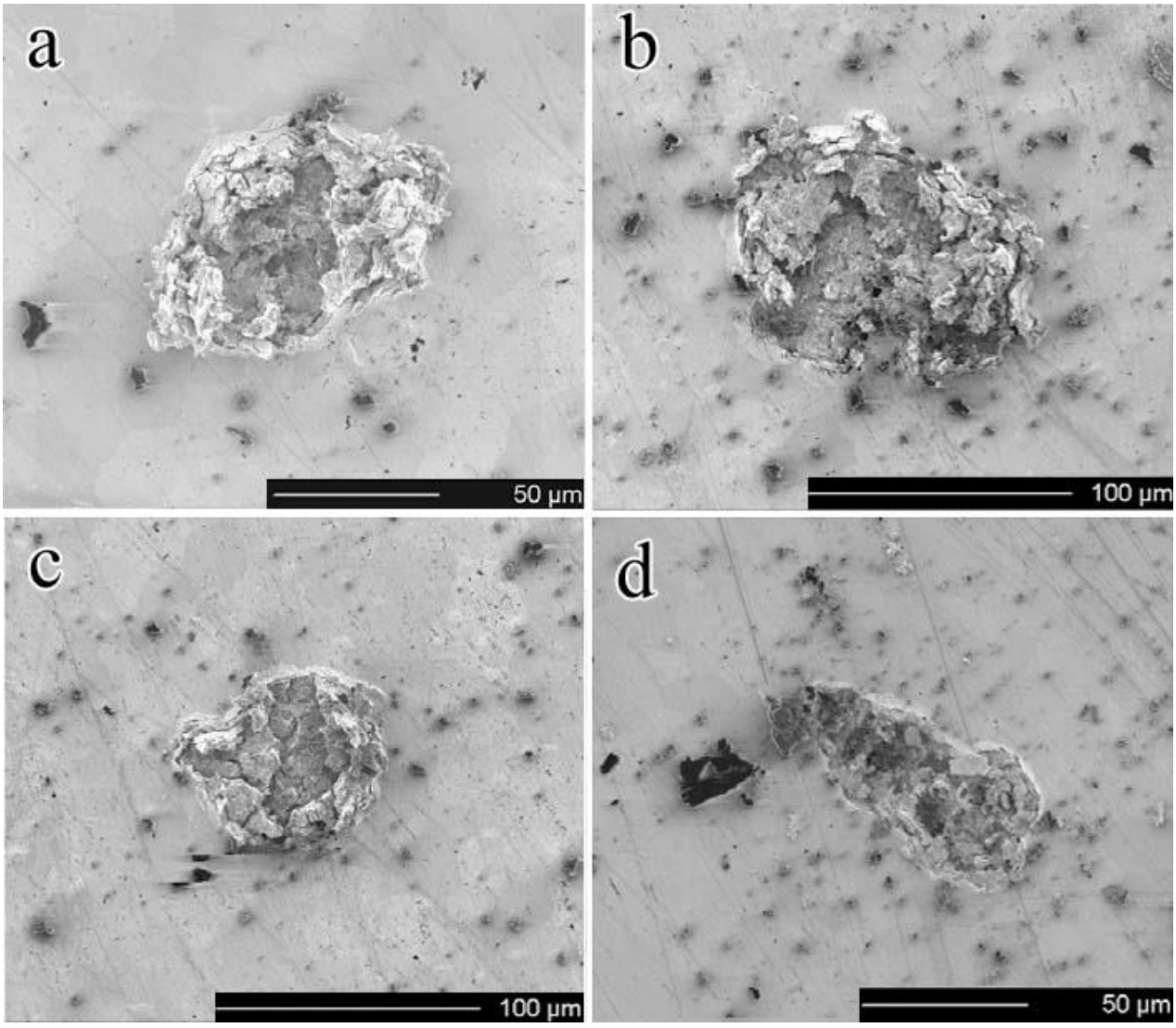

Figure 1 Focussed Ion Beam secondary electron images of hydrided low-carbon uranium illustrating the range in size and morphology of hydride formation via four selected examples. For each hydride, the volume expansion occurs both into and out of the metal, rupturing the existing oxide layer and spreading hydride debris across the surface.

Figure 2 SEM image of a mechanically sectioned hydride pit after the newly exposed face has been electropolished.

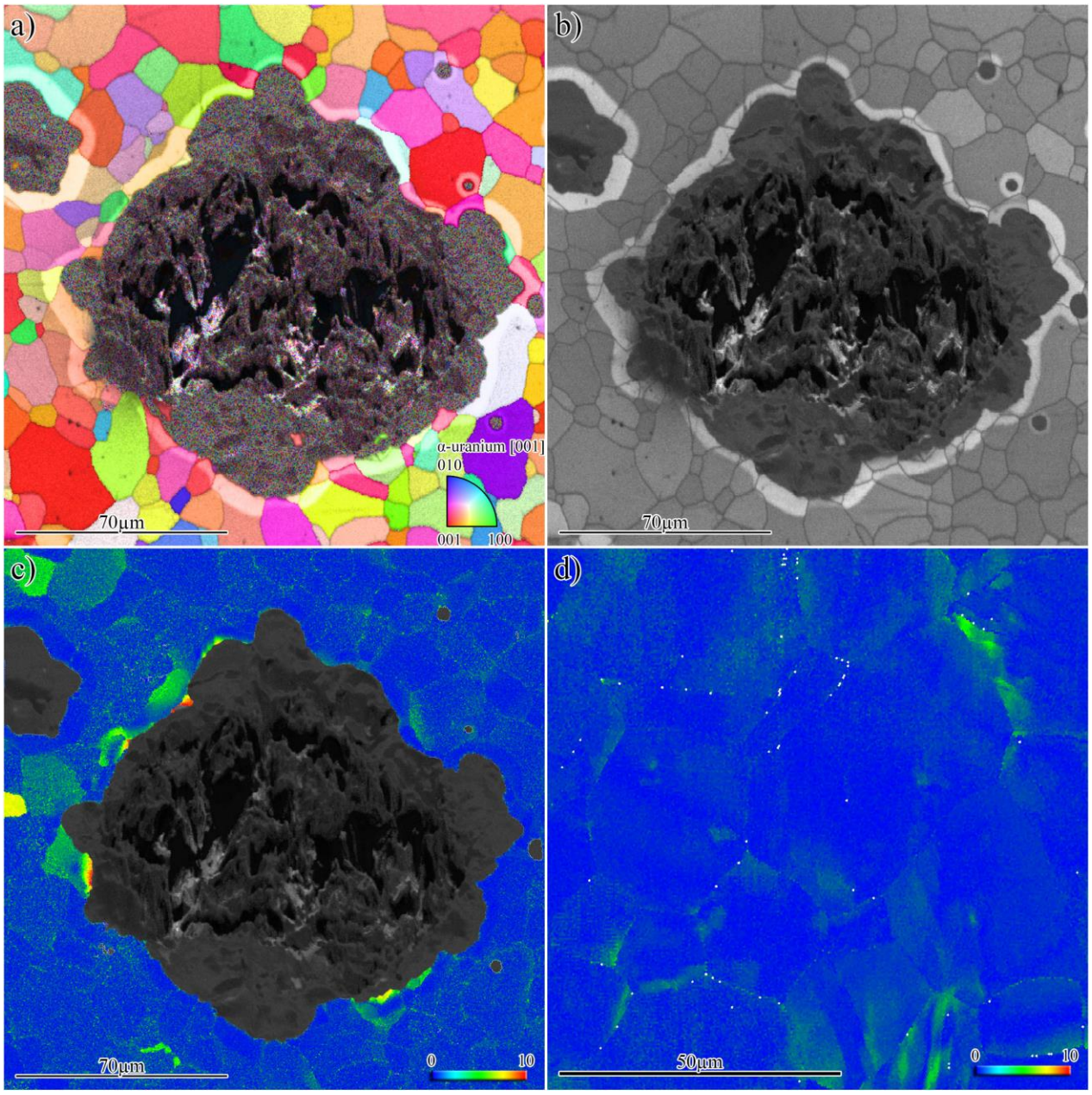

Figure 3 Scanning microscope images of a singular hydride location. The surface had been prepared by ion beam etching at an 80° incident angle to skim the surface free of any newly formed oxide. a) An inverse pole map from EBSD analysis shows the crystal orientation as a function of colour. The central hydride mass and occasional pitting from electropolishing appears black due to an absence of clear diffraction patterns. b) Secondary electron image quality map from the electron microscope. c) Crystal orientation variation map, the deviation from the average orientation is shown by a gradational colour change from blue (0°) through to red (10°). d) Crystal orientation variation map on an unreacted metal surface for comparison.

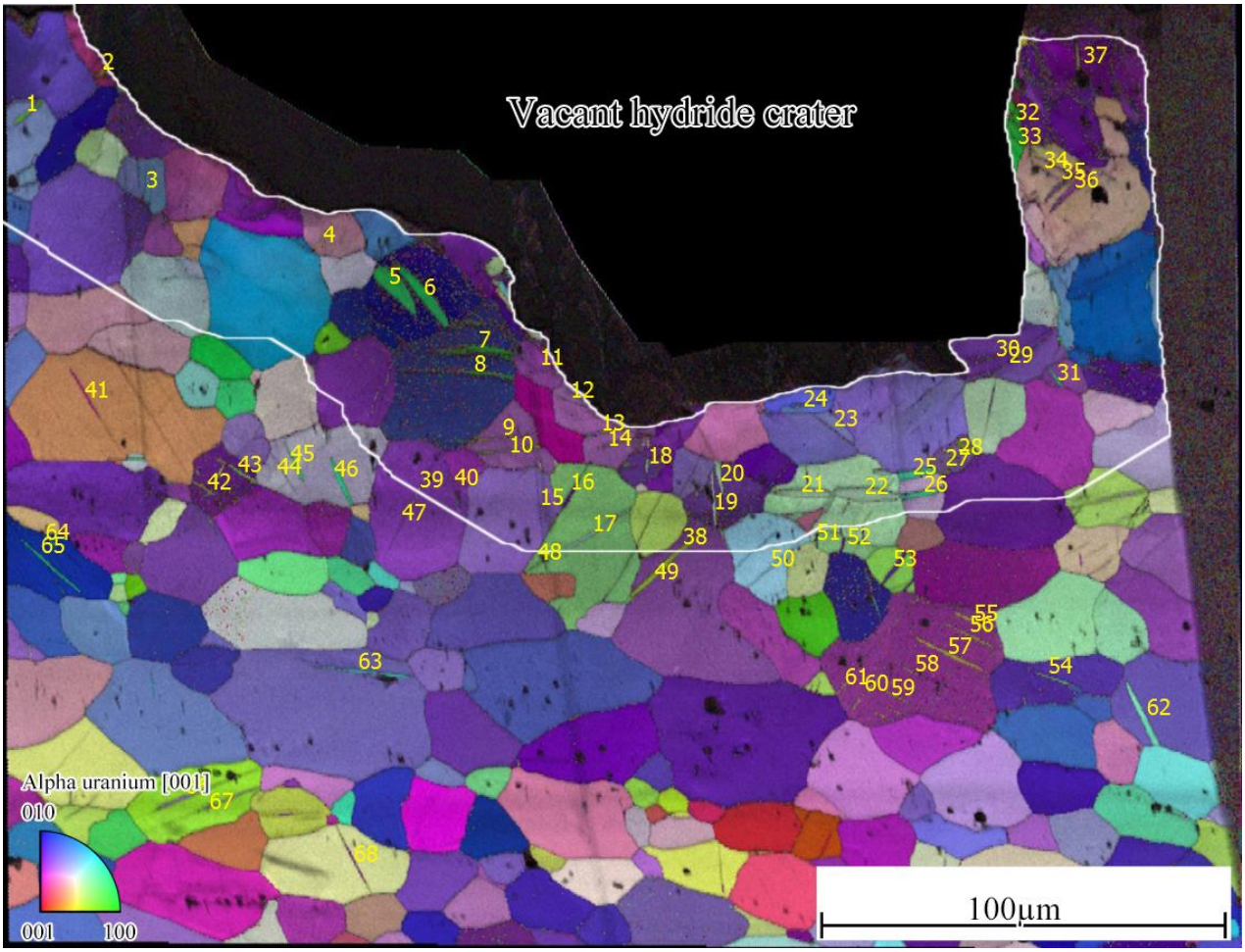

Figure 4 EBSD Inverse pole figure map of a section through a hydride growth, probing the crystalline microstructure beneath the reacted surface. The instances of twinning have been counted within a region 50µm from the edge of the hydride crater.

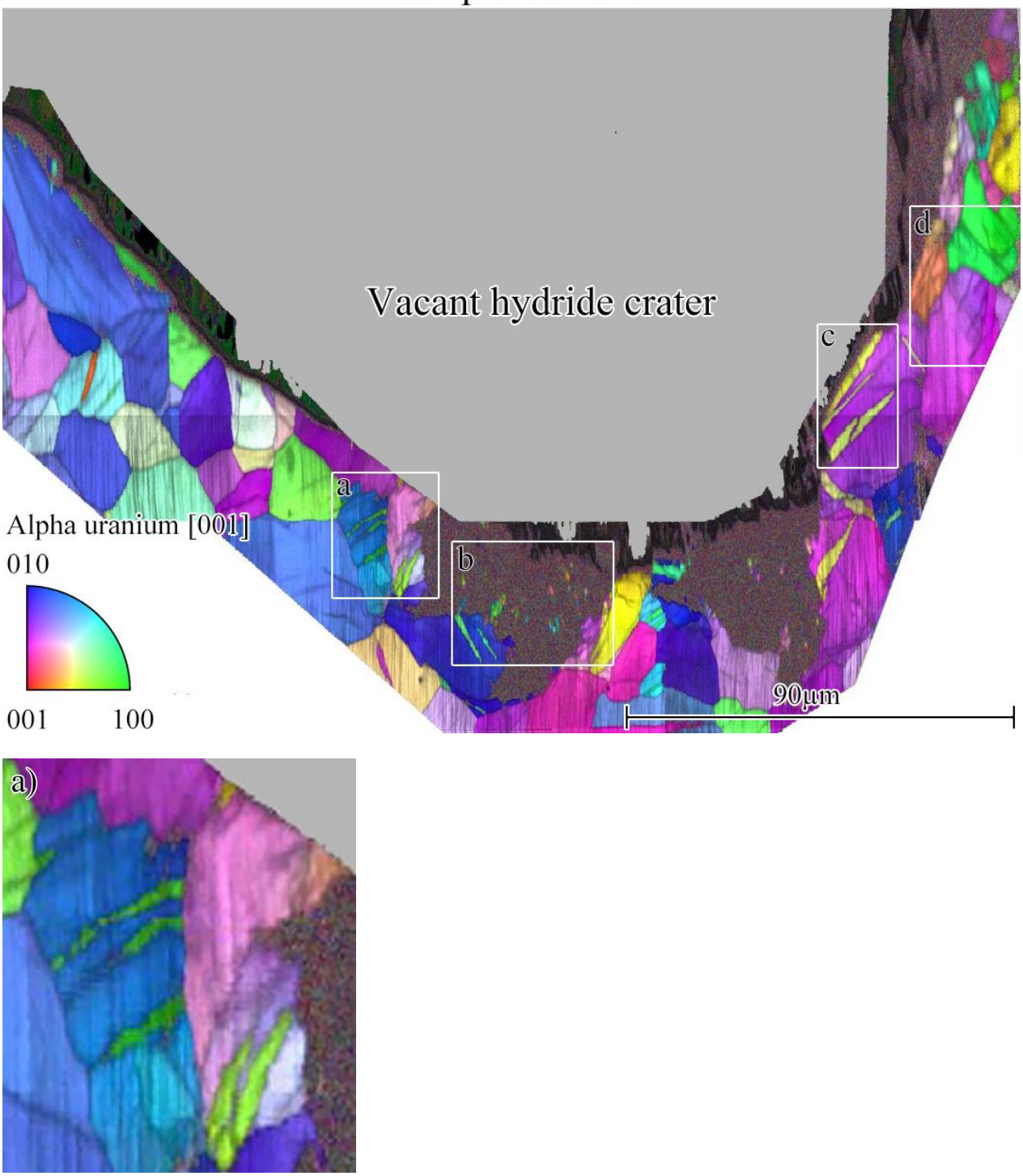
Sample Surface
Vacant hydride crater
a
b
c
d
Alpha uranium [001]
010
001
100
90µm
a)

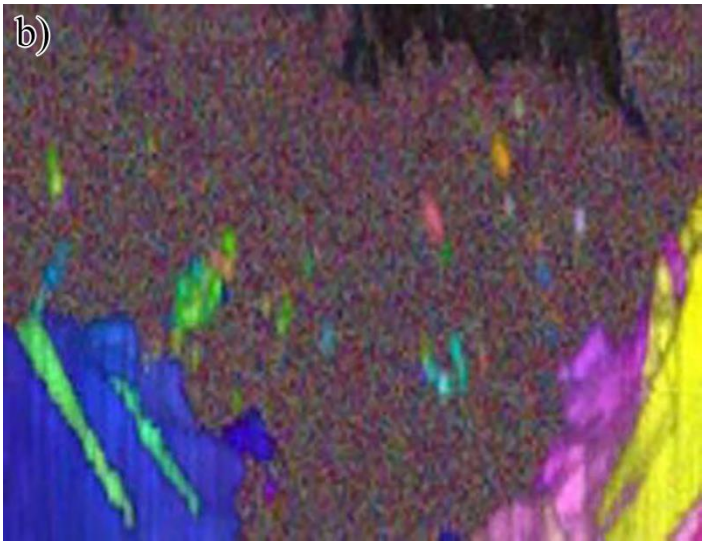
b)

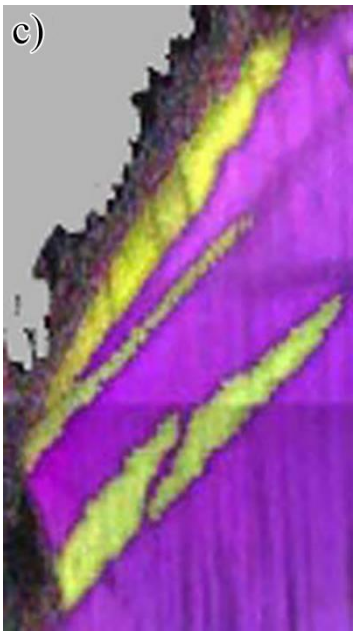
c)

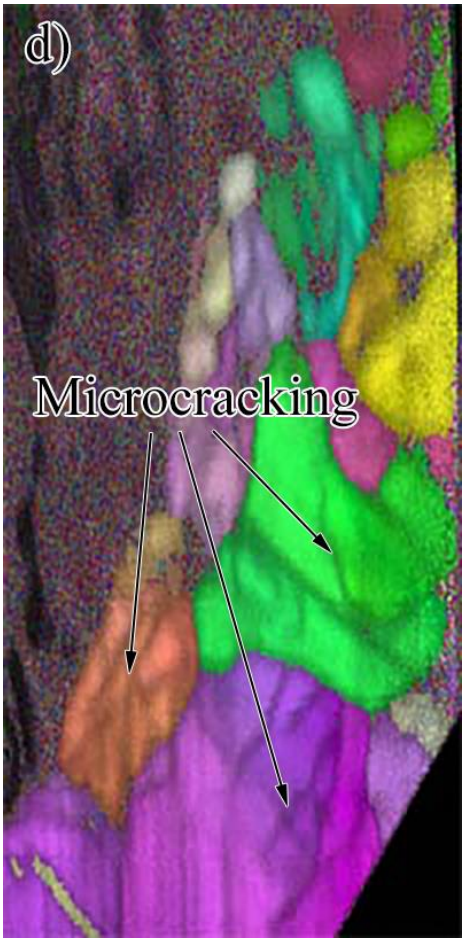

Figure 5 EBSD Inverse pole figure map of a FIB-cleaned section through a hydride growth, probing the crystalline microstructure beneath the reacted surface. Enlarged regions showing a) examples of stress-induced twinning adjacent to the hydride growth, b) fragmentation of uranium metal, c) twinning as the process of hydride consumption of the metal takes place and d) microcracking of the metal.

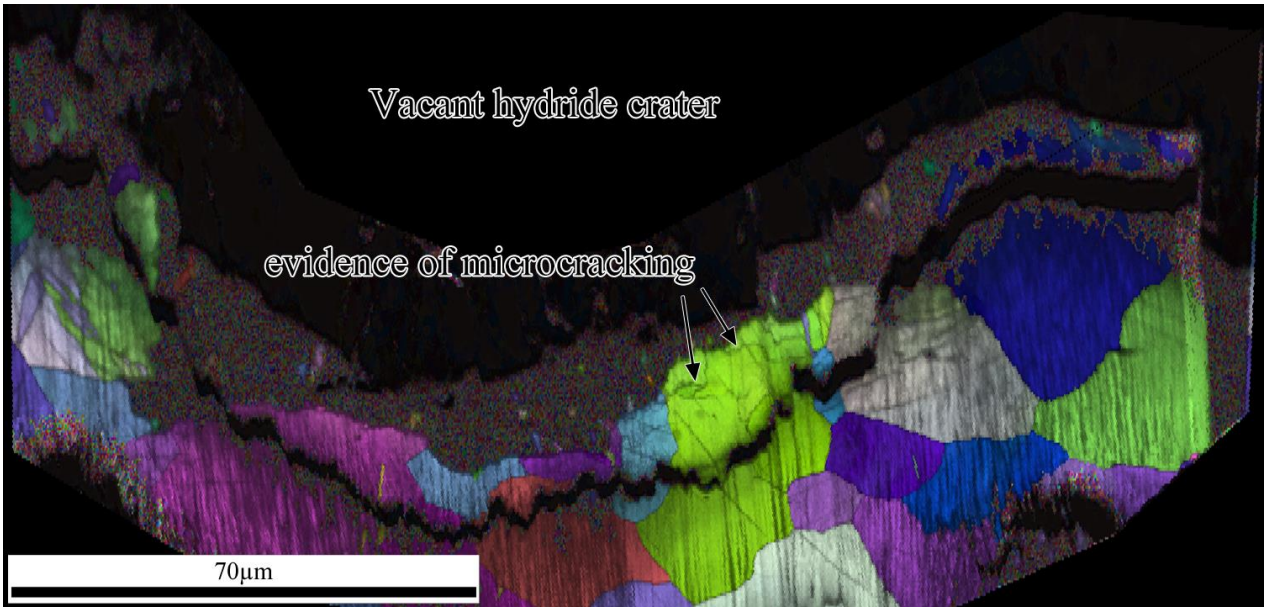

Figure 6 EBSD Inverse pole figure map of another FIB sectioned hydride growth utilising lower beam currents and less ion beam damage. The result shows clear evidence of microcracking in the immediate vicinity of the hydride edge.

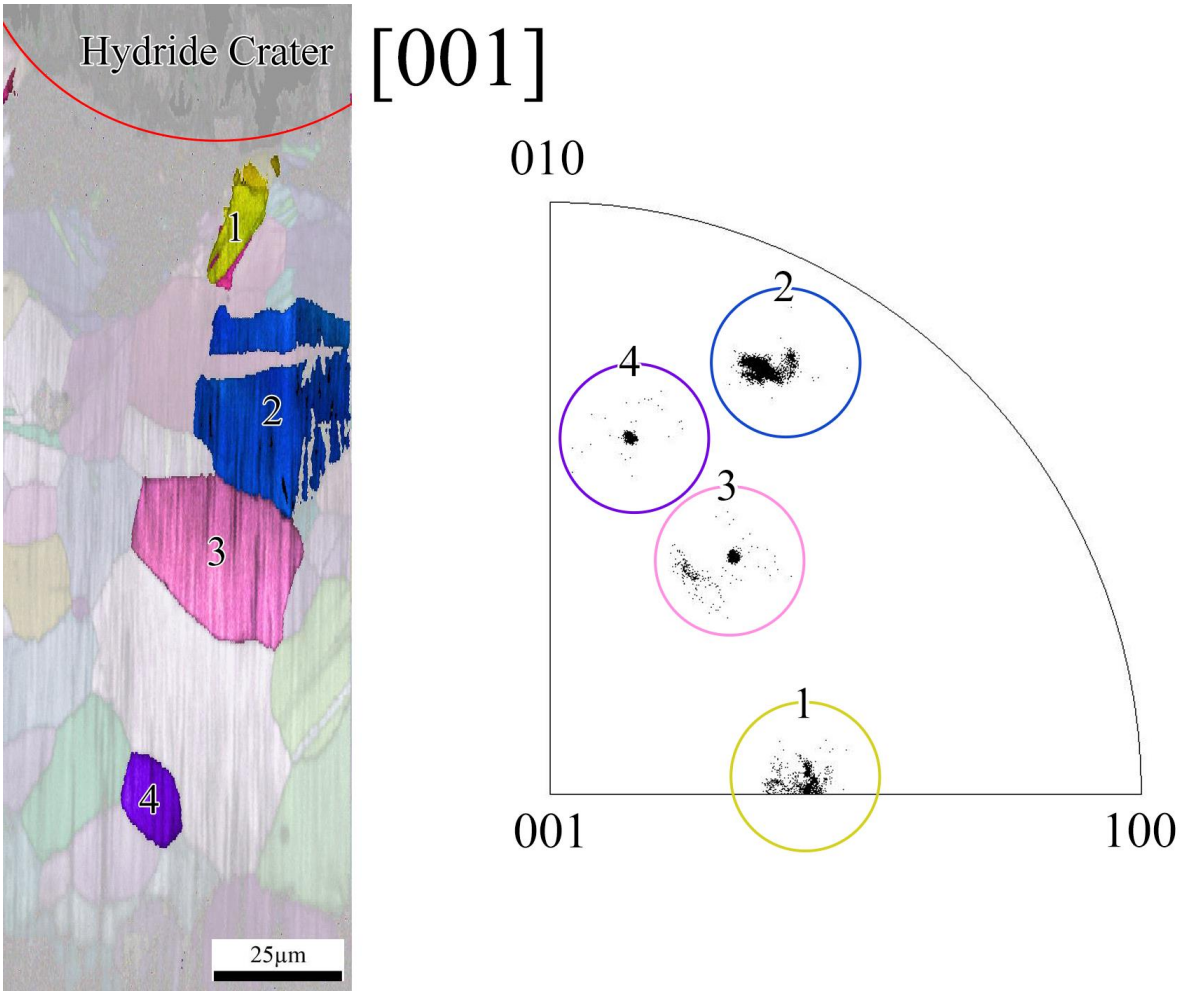

Figure 7 EBSD inverse pole figure map and combined SEM image (left) with inverse pole figure plot (right) of a section through the metal bordering on a hydride growth site. The highlighted grains are selected and analysed individually at varying distance from the corrosion growth. The grains closest to the hydride (1 and 2) have a more dispersed crystal orientation suggesting a large amount of strain. Metal grains further from the hydride (3 and 4) show comparably less strain with a highly congruent plot of crystal orientations. The hydride-metal boundary is indicated in red.